

# 3D Scanning by Means of Dual-Projector Structured Light Illumination

Ying Yu<sup>a</sup> and Daniel L. Lau<sup>a</sup>

<sup>a</sup>University of Kentucky, 453 F. Paul Anderson Tower, Lexington, KY 40506-0046, USA

## ABSTRACT

This paper introduces a dual-projector phase measuring profilometry that adds a second projector in a traditional structured light illumination system to improve the overall quality of the 3D scanning. With this method, two projectors are synchronized to a single camera, but each one projects structured light patterns of its unique frequency. The system performance benefits from a wider projection angle and a doubled light intensity. In particular, a detailed system implementation in hardware level is described. Moreover, the major difference between the phase unwrapping of dual-projector system and the single-projector system is discussed, and a LUT-based phase unwrapping scheme for this dual-projector phase measuring profilometry system is proposed.

**Keywords:** Structured light illumination, phase measuring profilometry, dual-projector, phase unwrapping

## 1. INTRODUCTION

As one of the non-contact 3D shape measurement techniques, the structured light illumination (SLI) has been known for its high resolution and high speed.<sup>1</sup> Conventional SLI systems consist of one projector, one camera and one processing unit which is usually a computer. The projector presents patterns that are encoded with some information related to the pixel locations on the object to be measured. If the projection is on a flat surface, the patterns seen should be identical to its original design. However, with the presence of the non-planar object under the projection, what is actually seen from the camera is the distorted patterns on the surface of the object. By comparing and analyzing the distortion in the images taken by the camera, the 3D surface of the object can eventually be reconstructed in a processing unit.

Within the scope of this fundamental idea and system structure, a lot of research has been done over the past several decades.<sup>2</sup> Different practical implementations have been proposed, from pattern design to system calibration, then to the algorithms that are used to decode the captured patterns. One widely studied area is the one-shot SLI strategy in which only one static pattern is projected onto the object. It employs color pattern,<sup>3</sup> binary grid pattern,<sup>4</sup> gray-scale pattern<sup>5</sup> or even composite pattern.<sup>6</sup> Since there is only one image need to be processed for a scan, the 3D reconstruction can be completed fast. The one-shot strategy is ideal for high speed applications such as real time scanning. But in terms of accuracy, it is not so promising compared to some multi-shot SLI strategy in which the 3D reconstruction is derived by projecting a sequence of patterns and processing multiple images.<sup>7</sup>

According to the method of encoding the information containing the pixel location into the pattern, phase measuring profilometry (PMP)<sup>8</sup> is a subset of SLI techniques that acquires the depth value by translating the phase data from the projected patterns pixelwise. The PMP has some advantageous features including its insensitivity to ambient light and its high accuracy.<sup>9,10</sup> Higher frequency patterns have been introduced to PMP systems to reduce the effects of the noise and achieve higher accuracy.<sup>11</sup> Nonetheless, higher frequency patterns also produces the phase ambiguity which requires the system to execute some extra computation called phase unwrapping.<sup>12</sup> Furthermore, adding high frequency patterns increases the projection time as well as the number of images to be processed, which accordingly decreases the overall speed of the system. Liu *et al.* proposed an ingenious dual-frequency pattern strategy which combines a high-frequency pattern and a unit-frequency pattern into one composite pattern,<sup>13</sup> it improved the accuracy without increasing the scanning time.

---

Further author information: (Send correspondence to Daniel L. Lau)

Daniel L. Lau: E-mail: dllau@uky.edu, Telephone: 1 859 257 1787

Ying Yu: E-mail: yyu226@g.uky.edu

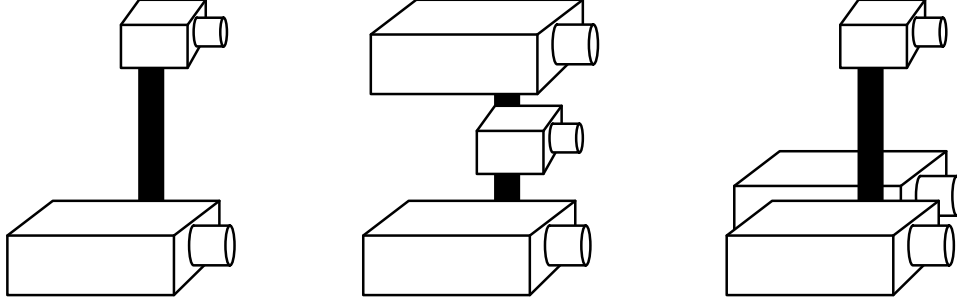


Figure 1: Structured light scanners composed of (left) a single projector, (center) opposed dual-projectors for wrap around scanning, and (right) complementary dual-projectors for increased luminance.

In this paper, we propose a dual-projector, dual-frequency SLI scheme and its practical implementation. Unlike the scanner presented by Jiang *et al.*,<sup>14</sup> the proposed scanner projects patterns from both projectors simultaneously, which keeps the scan time the same versus a single projector scanner. We also allow the projectors to be placed in any arbitrary arrangement with 3D point clouds generated from a single fused phase image instead of fusing to independently generated point clouds. Depending on the arrangements of projectors as illustrated in Fig. 1, a dual-projector SLI scanner can be used to minimize occlusions<sup>15</sup> since a scan surface needs to be visible to at least one projector and the camera. So placing projectors in opposition means a face, for example, can be illuminated from both sides. Having two unique paths of light from projector to camera also creates new opportunities and challenges for overcoming the issue of multi-path.<sup>16</sup> Placing projectors side-by-side can be used to achieve twice the luminance of a single projector. Higher light intensity gives rise to the higher signal-to-noise ratios (SNR),<sup>17</sup> which makes the system less susceptible to sensor noise, consequently the system becomes more robust and accurate.

Now in order for dual-projector SLI scanners to become practical, there are two fundamental problems that need to be addressed. The first is the practical implementation of control logic to perfectly synchronize the projectors to a camera. For this, we describe an FPGA-based controller using a commodity FPGA board to simultaneously drive two HDMI ports. The advantage of this system is that it allows us to avoid the practical issues associated with modern GPUs as well as staying low cost. The second problem that needs to be addressed is how to perform phase unwrapping when the phase images derive from separate projectors arbitrarily arranged. Using the dual-frequency pattern scheme, we demonstrate using a unit-frequency phase image from one projector to unwrap the high-frequency phase image in the second, opposed projector, using a look-up table-based operation ideally suited for GPUs. This real-time approach is highly flexible and can be used to replace phase unwrapping schemes such as the Chinese remainder technique of Xia *et al.*<sup>18</sup>

## 2. DUAL-FREQUENCY PHASE MEASURING PROFILOMETRY

The dual-frequency pattern scheme was initially proposed by Liu *et al.*,<sup>13</sup> it is essentially an improved derivation of the phase measuring profilometry.<sup>10</sup> In the traditional PMP, a series of phase-shifting sinusoidal fringe patterns are projected onto the object to be measured. The fringe patterns can be either horizontal or vertical such that the presence of the object distorts the patterns where by analyzing the phase values in the deformed pattern images, the 3D depth values can be obtained.

Suppose the phase-shifting patterns are vertical, which indicates that all the pixels in a same row have the identical intensity, and from top to bottom the value of intensities in each row form a sinusoidal function. Therefore, this kind of PMP patterns can be generalized as:

$$I_n^p(x^p, y^p) = A^p + B^p \cos \left( 2\pi f y^p - \frac{2\pi n}{N} \right), \quad (1)$$

where  $I_n^p$  is the intensity of the pixel at the coordinate  $(x^p, y^p)$  from the projector's point of view;  $A^p$  is background intensity which is considered as a constant;  $B^p$  is another constant which represents the fringe contrast compared

to the background;  $f$  is the frequency of the fringe pattern set which is equal to the number of sinusoidal periods from top to the bottom of the projected patterns;  $N$  is the total number of the phase-shifting patterns of the same frequency in a set,  $n$  is the current number of the pattern within the range of  $[0, N - 1]$ .

On the camera's side, the image of the object under the projection of each unique PMP pattern is captured as part of the data to reconstruct the 3D profile of the object. So the projected scene of the object can be described as Eq. (2) from the camera's point of view,

$$I_n^c(x^c, y^c) = A^c(x^c, y^c) + B^c(x^c, y^c) \cos\left(\phi(x^c, y^c) - \frac{2\pi n}{N}\right), \quad (2)$$

where  $I_n^c$  is the intensity of the given pixel  $(x^c, y^c)$  in the camera's coordinates system;  $A^c(x^c, y^c)$  is the average intensity of the given pixel over the  $N$  patterns;  $B^c$  can be considered as the average intensity of the PMP pattern seen by the camera. So for any given pixel  $(x^c, y^c)$  in a pattern set  $[0, N - 1]$ ,  $A^c$  and  $B^c$  are both constant; furthermore,  $B^c(x^c, y^c)$  can be derived from Eq. (2) as:

$$B^c(x^c, y^c) = \frac{2}{N} \sqrt{\left[\sum_{n=0}^{N-1} I_n^c(x^c, y^c) \sin\left(\frac{2\pi n}{N}\right)\right]^2 + \left[\sum_{n=0}^{N-1} I_n^c(x^c, y^c) \cos\left(\frac{2\pi n}{N}\right)\right]^2}. \quad (3)$$

In Eq. 2, there is another important constant  $\phi$  for any given pixel  $(x^c, y^c)$  in a given pattern set  $[0, N - 1]$ , it is the phase value  $\phi(x^c, y^c)$  of the distorted fringe patterns that is eventually used to calculate the corresponding depth value of the object. The expression of  $\phi(x^c, y^c)$  can be inferred from Eq. (3) as:

$$\phi(x^c, y^c) = \frac{1}{2\pi} \left( \arctan \frac{\sum_{n=0}^{N-1} I_n^c(x^c, y^c) \sin(\frac{2\pi n}{N})}{\sum_{n=0}^{N-1} I_n^c(x^c, y^c) \cos(\frac{2\pi n}{N})} + \pi \right), \quad (4)$$

where the  $\arctan(\cdot)$  range of  $[-\pi, \pi]$  is transformed to the phase value,  $\phi(x^c, y^c)$ , in the range of  $[0, 1]$ .

The dual-frequency pattern scheme adds a second sinusoidal component to the phase-shifting patterns. As a result, the total number of patterns is still  $N$ , but each pattern has two sinusoidal components. One is of unit frequency  $f_u$  while the other is of a high frequency  $f_h$  that is used to reduce the impact of noises in the system. If we extend the single-frequency PMP pattern above to the dual-frequency, the intensities of the row pixels from top to bottom would be like an amplitude modulation in which the  $f_u$  is frequency of the modulating signal and  $f_h$  is the frequency of the carrier wave. According to Liu *et al.*, from the projector's point of view, the new dual-frequency pattern is expressed as:

$$I_n^p(x^p, y^p) = A^p + B_1^p \cos\left(2\pi f_h y^p - \frac{2\pi n}{N}\right) + B_2^p \cos\left(2\pi f_u y^p - \frac{4\pi n}{N}\right), \quad (5)$$

where the  $I_n^p$  is the intensity of the pixel  $(x^p, y^p)$  in the  $n^{th}$  pattern. Similarly, the intensity equation of the camera coordinates used for reconstruction becomes:

$$I_n^c(x^c, y^c) = A^c(x^c, y^c) + B_1^c(x^c, y^c) \cos\left(\phi_h(x^c, y^c) - \frac{2\pi n}{N}\right) + B_2^c(x^c, y^c) \cos\left(\phi_u(x^c, y^c) - \frac{4\pi n}{N}\right). \quad (6)$$

Likewise, the  $B_1^c$ ,  $B_2^c$  and  $\phi_h$ ,  $\phi_u$  can be derived from Eq. (3) and Eq. (4) respectively,

$$B_m^c(x^c, y^c) = \frac{2}{N} \sqrt{\left[\sum_{n=0}^{N-1} I_n^c(x^c, y^c) \sin(m \frac{2\pi n}{N})\right]^2 + \left[\sum_{n=0}^{N-1} I_n^c(x^c, y^c) \cos(m \frac{2\pi n}{N})\right]^2}, \quad (7)$$

where  $m = 1$  or  $2$  in this case,

$$\phi_h(x^c, y^c) = \frac{1}{2\pi} \left( \arctan \frac{\sum_{n=0}^{N-1} I_n^c(x^c, y^c) \sin(\frac{2\pi n}{N})}{\sum_{n=0}^{N-1} I_n^c(x^c, y^c) \cos(\frac{2\pi n}{N})} + \pi \right) \text{ and} \quad (8)$$

$$\phi_u(x^c, y^c) = \frac{1}{2\pi} \left( \arctan \frac{\sum_{n=0}^{N-1} I_n^c(x^c, y^c) \sin(\frac{4\pi n}{N})}{\sum_{n=0}^{N-1} I_n^c(x^c, y^c) \cos(\frac{4\pi n}{N})} + \pi \right). \quad (9)$$

where, again,  $\phi_h$  and  $\phi_u$  are scaled to the range  $[0, 1]$ . However, the actual range of  $\phi_h$  is  $[0, f_h]$  – so  $\phi_h$  is called the wrapped phase. Unwrapping the  $\phi_h$  to  $\tilde{\phi}_h \in [0, f_h]$  can lead to a more accurate conversion from phase to depth. In order to obtain  $\tilde{\phi}_h$ , the value of  $\phi_u$  is used as the following equation shows,

$$\tilde{\phi}_h(x^c, y^c) = (\phi_h(x^c, y^c) + \lfloor f_h \phi_u(x^c, y^c) - \phi_h(x^c, y^c) + 0.5 \rfloor) / f_h, \quad (10)$$

where the  $\lfloor \cdot \rfloor$  is the symbol of floor function which outputs the greatest integer less than or equal to the value enclosed.

Now that we have unambiguous, unwrapped phase term,  $\tilde{\phi}_h$ , we can derive the 3D point from our scan according to Liu *et al.*<sup>13</sup>

$$Z^w = M_z(x^c, y^c) + \frac{N_z(x^c, y^c)}{C(x^c, y^c)\tilde{\phi}_h(x^c, y^c) + 1}, \quad (11)$$

$$X^w = E_x(x^c, y^c)Z^w + F_x(x^c, y^c), \quad (12)$$

$$Y^w = E_y(x^c, y^c)Z^w + F_y(x^c, y^c). \quad (13)$$

where the coefficients  $M_z(x^c, y^c)$ ,  $N_z(x^c, y^c)$ ,  $E_x(x^c, y^c)$ ,  $E_y(x^c, y^c)$ ,  $F_x(x^c, y^c)$ ,  $F_y(x^c, y^c)$  and  $C(x^c, y^c)$  are determined, for each individual camera pixel, during calibration of the projector and cameras lenses, assuming pin-hole lens models.

### 3. DUAL-PROJECTOR PHASE MEASURING PROFILOMETRY

In this paper, we apply the dual-frequency PMP to a dual-projector system in which the SLI patterns in Eq. (5) are jointly generated by two separate projectors H and U. The projector H produces the high frequency ( $f_h$ ) component while the projector U only produces the unit frequency ( $f_u$ ) component. Thus, their intensity equations can be expressed as:

$$I_n^{p_h}(x^{p_h}, y^{p_h}) = A^{p_h} + B_1^{p_h} \cos\left(2\pi f_h y^{p_h} - \frac{2\pi n}{N}\right), \text{ and} \quad (14)$$

$$I_n^{p_u}(x^{p_u}, y^{p_u}) = A^{p_u} + B_2^{p_u} \cos\left(2\pi f_u y^{p_u} - \frac{4\pi n}{N}\right), \quad (15)$$

respectively. During the reconstruction process, Eqn. (6) and (9) remain the same; however, Eqn. (10) is not applicable for the dual-projector system since the two phases do not have a deterministic relationship. Instead, we use a lookup table (LUT) to acquire the unwrapped phase according to:

$$\tilde{\phi}_h(x^c, y^c) = (\phi_h(x^c, y^c) + \lfloor LUT[x^c, y^c, \phi_u(x^c, y^c)] - \phi_h(x^c, y^c) + 0.5 \rfloor) / f_h, \quad (16)$$

where the look-up table,  $LUT[x^c, y^c, \phi_u(x^c, y^c)]$ , represents a 3D matrix that is populated from the data collected during calibration.

The procedure for calibrating our scanner is illustrated in Fig. 2 and involves sweeping a rigid, flat checkerboard pattern in correspondence with the  $XY$ -plane and moving in fixed, small-steps through the scan volume from the nearest plane where  $Z = Z_{min}$  to the farthest plane at  $Z = Z_{max}$ . The physical moving of the checkerboard pattern is performed using a motorized rail like the Velmex Bi-slide and VXM controller. These rails can be configured to move with a positional accuracy of 0.076 mm and repeatability of 0.005 mm. The specific checkerboard pattern that we use the CalTag calibration target introduced by Atcheson *et al.*<sup>19</sup> where, inside each square, is a unique 16-bit codeword identifying and absolute world ( $X_w, Y_w$ ) coordinates of each squares four corners.

As stated above, the calibration procedure involves iteratively moving the CalTag target along the  $Z$ -axis from  $Z_{min}$  to  $Z_{max}$  such that, at each step, we perform a structured light scan with each camera pixel defined according to:

$$I_c[x^c, y^c, k] = [X_w[x^c, y^c, k], Y_w[x^c, y^c, k], Z_w[x^c, y^c, k], P_h[x^c, y^c, k], P_u[x^c, y^c, k]] \quad (17)$$

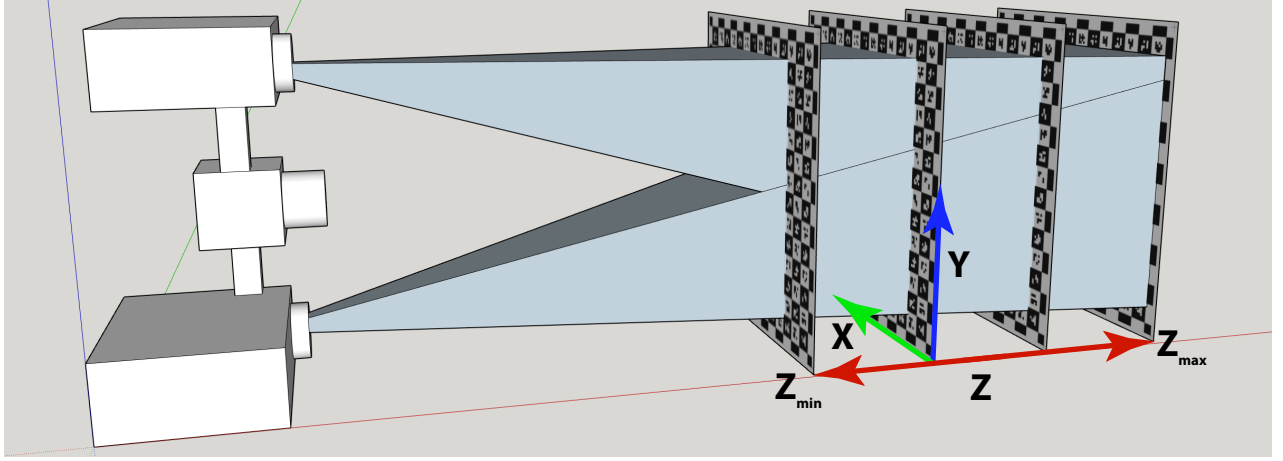


Figure 2: Illustration showing dual-projector scanner calibration.

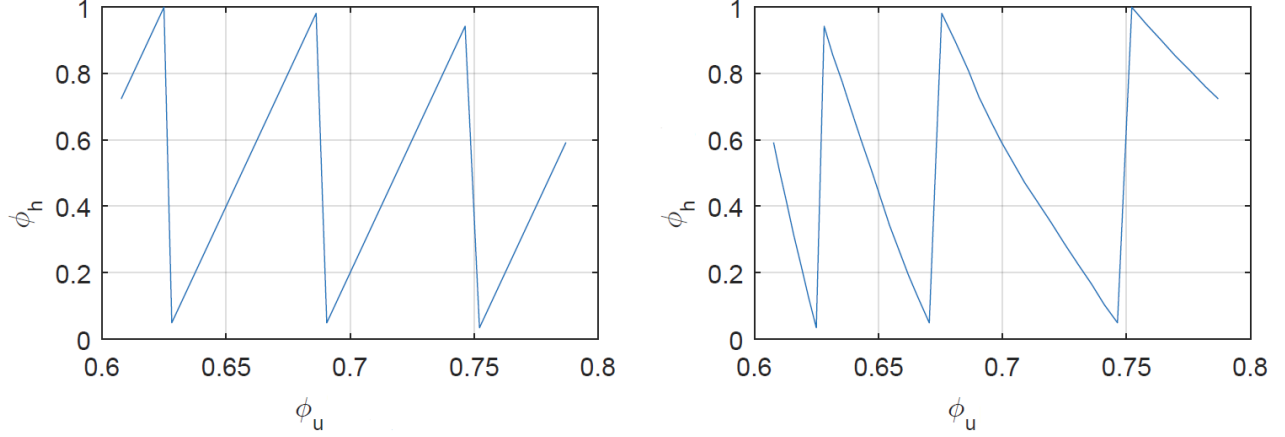


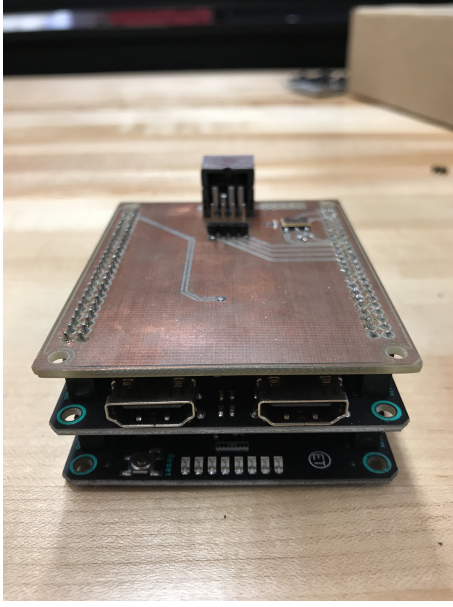
Figure 3:  $\phi_f$  vs.  $\phi_u$  in single-projector system (left) and dual-projector system (right)

where  $x^c$  and  $y^c$  are the pixel's column and row coordinates;  $k$  is the step index for the current scan;  $X_w[x^c, y^c, k]$  and  $Y_w[x^c, y^c, k]$  are the CalTag grid coordinate at the intersection of the CalTag target's surface and the camera pixel's line-of-sight;  $Z_w[x^c, y^c, k]$  is the Z-position of the rail; and  $P[x^c, y^c, k]$  is the phase value of the projected PMP sequence in the line-of-sight of the camera pixel. Once complete, we then have a 3D texture composed of a stack of 4-color digital images that are the height and width of our camera and  $K$  layers deep with  $P[x^c, y^c, k]$  ranging from  $P_{min}[x^c, y^c]$  to  $P_{max}[x^c, y^c]$  as  $Z_w[x^c, y^c, k]$  ranges from  $Z_{min}[x^c, y^c]$  to  $Z_{max}[x^c, y^c]$ .

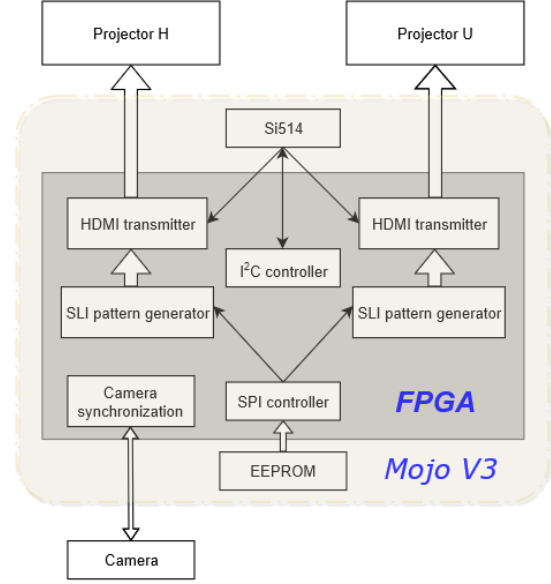
Fig. 3 illustrates the relationship between the  $\phi_f$  and  $\phi_h$  for the single-projector PMP system (left) and the dual-projector PMP system (right) respectively.

#### 4. SYSTEM IMPLEMENTATION

Our FPGA-based dual-projector Structured Light Illumination (SLI) system generates two synchronized SLI patterns which are then fed to two projectors via HDMI. Meanwhile, the projectors and the camera need to be synchronized to ensure that the camera images are taken at the right timing. A photo of our system and the system diagram are shown in Fig. 4a and Fig. 4b. The two SLI pattern generators output two synchronized phase-shifting fringe patterns which are later encoded into TMDS data streams by the HDMI transmitters and eventually move to projectors.



(a) A photo of the system



(b) System diagram

Figure 4: Our dual-projector system

HDMI is the abbreviation of High-Definition Multimedia Interface, it is one of the most popular display interfaces. The newest release, HDMI Version 2.1 supports up to 10K video at 120Hz. A standard HDMI connector has 19 pins,<sup>20</sup> Data channel 2, 1, 0 are mainly used to transfer red, green and blue components of the video respectively. The HDMI does not only transfer video data, but also some auxiliary data, for example audio data, packet header. The auxiliary data, video data as well as some control signals are encoded in data channel 2, 1, 0 and then digitally transmitted in serial. In between any two adjacent video periods, one or more data island period and control period are inserted.

In HDMI, there are six important control signals, HSYNC indicates the beginning and end of a row in a frame of the video, VSYNC indicates the beginning and end of a frame, CTL0 CTL3 indicate the data type of the following data period. The three data channels are transmitted through a differential signaling technology called Transition-Minimized Differential Signaling (TMDS) to reduce the impact of electromagnetic interference and enable high clock skew tolerance.

The 5 volts power signal is provided by the HDMI source or an external source, which after the HDMI sink reads the 5 volts signal, it immediately asserts the pin, Hot Plug Detect. Once the HDMI source detects the presence of a sink by the assertion of the pin Hot Plug Detect, it sends an  $I^2C$ -based command of a read request to the sink. The pins SCL and SDA compose the display data channel (DDC) via which the Extended Display Identification Data (EDID) is read by the HDMI source from the sink as the response to the read request. The EDID is usually 128 or 256 bytes long, it contains various information related to the features of display system, including but not limited to, manufacturer ID, serial number, week and year of manufacture, screen size, supported timing, etc.

The pin CEC is used to add some advanced functionalities for the HDMI systems. Usually it is a remote control that issues different high-level commands to the devices connected by HDMI cables. CEC stands for Consumer Electronics Control, it is also a one-wire bus protocol, the implementation of CEC is optional, because not all the HDMI devices support this feature. Since HDMI 1.4, the previously reserved pin has become the HDMI Ethernet and Audio Return Channel (HEAC). While it is in audio return channel mode, only the HEAC+ line is used to transmit audio data; in HDMI Ethernet channel mode, the HEAC+ line pairs up with the HEAC- line as a differential signal to establish a high speed Ethernet communication.

To obtain the uncommon 73.25 MHz pixel clock for  $800 \times 600$  pixel video at 120 Hz which cannot be generated

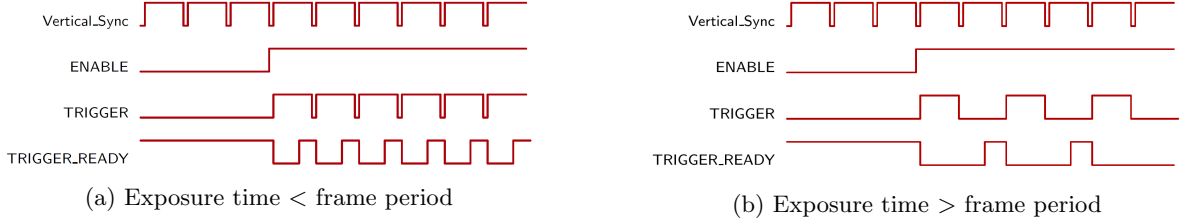


Figure 5: Timing diagram of the camera's IO signals

by the Spartan 6 of the Mojo board, we utilize a programmable oscillator, the Si514. By configuring the internal registers through  $I^2C$  bus, Si514 can generate any frequency from 100 kHz to 250 MHz with a tuning resolution of 0.026 ppb. Therefore, an  $I^2C$  master controller was incorporated into the system.

Now in order to linearize the projector to avoid the deleterious effects of gamma distortion<sup>21</sup> on our projected PMP patterns, we use the EEPROM on the Mojo board to upload calibrated tone correction curves for our target projector. This LUT can be hard-coded into the configuration file of the FPGA, but the drawback is that once the lookup table changes, the FPGA configuration file has to be changed. It is quite inconvenient especially when the system needs to be often applied to a different projector, because generating a new FPGA configuration file requires special development tool and takes more time. We devise an approach that the user stores the LUT in a separate EEPROM chip which can be erased and written by any computer via some general serial or USB tools, and the SPI master module in the FPGA reads the EEPROM every time the system is powered on. With this approach, users can load new LUTs much faster and easier.

The camera synchronization module not only controls the timing of the camera trigger, but also monitors the status of the camera. There are three wires that link the camera and the FPGA, they are *ENABLE*, *TRIGGER* and the *TRIGGER\_READY*. The *ENABLE* and *TRIGGER\_READY* are output signals from the camera, which are programmable from the PC connected to the camera. The *TRIGGER* is an input signal to the camera that is controlled by the FPGA. Initially, the camera pulls the *ENABLE* high to tell the FPGA that a new scan is about to start, so the FPGA sends the first SLI pattern to the projector. Meanwhile, the rising edge of the *Vertical\_Sync* from HDMI module is passed to the *TRIGGER*, it is this rising edge that triggers the camera's first exposure. During the exposure time, the *TRIGGER\_READY* is pulled low, which indicates the FPGA that no more triggers should be issued for the camera, because the camera is busy processing the current exposure and not ready for the next shot. Likewise, the projector should keep displaying the same SLI pattern. Once an exposure is done, the *TRIGGER\_READY* immediately goes high, which tells the FPGA that the camera is ready for another exposure, so the rising edge of the following *Vertical\_Sync* can be sent to *TRIGGER* and the next SLI pattern can be sent to the projector. From the PC side, the *TRIGGER\_READY* is programmed by setting different values to the camera's parameters such as trigger delay and exposure time. Fig. 5 briefly illustrates the synchronization between the camera and the projectors. If the exposure time is shorter than the frame period of the projectors, every pulse of the *Vertical\_Sync* is transmitted to trigger the camera as shown in 5a; on the contrary if the exposure time is greater than the frame period, only one out a few *Vertical\_Sync* is transmitted to *TRIGGER*. The Fig. 5b shows the case in which  $frame\ period < exposure\ time < 2 \times frame\ period$ , every other *Vertical\_Sync* is used as trigger.

## 5. CONCLUSIONS

In this paper, we have introduced a generalized frame work for building multi-projector structured light scanners. Specifically, we have developing an FPGA controller to drive two synchronized projectors with camera hand-shaking such that the projected pattern sequences run at an adjustable frame rate regulated by the camera's acquisition speed. In addition to this hardware, we have also introduced a pattern scheme that allows multiple patterns to be superimposed on each other and separated by the processing of the captured images inside the CPU. This disambiguation allows the projectors to be assembled in any arbitrary arrangement. And using our described calibration technique, we can fuse the phase images from multiple projectors to acquire a cohesively fused phase image from which to derive depth. Future research will focus on integrating the FPGA engine inside

the FPGA resources of an existing machine vision camera to create a camera that converts any HDMI projector into an instant structured light scanner.

## ACKNOWLEDGMENTS

This work has been supported by Intel Corporation and the National Science Foundation under contract No. 1539157 and the Visual and Experiential Computing initiative. Dr. Daniel L. Lau is a Professor at the University of Kentucky and a Founder of Seikowave Inc., a private company that designs and sells structured light scanners.

## REFERENCES

1. Chen, F., Brown, G. M., and Song, M., "Overview of three-dimensional shape measurement using optical methods," *Opt. Eng.* **39**, 10–22 (2000).
2. Geng, J., "Structured-light 3d surface imaging: a tutorial," *IEEE Intelligent Transportation System Society* (31 March 2011).
3. Wust, C. and Capson, D. W., "Surface profile measurement using color fringe projection," *Machine Vision and Applications* **4**, 193–203 (1991).
4. Grin, P. M., Narasimhan, L. S., and Yee, S. R., "Generation of uniquely encoded light patterns for range data acquisition," *Pattern Recog.* **25**(6), 609–616 (1992).
5. Durdle, N. G., Thayyoor, J., and Raso, V. J., "An improved structured light technique for surface reconstruction of the human trunk," *IEEE Canadian Conference of Electrical and Computer Engineering* **2**, 874–877 (1998).
6. Guan, C., Hassebrook, L. G., Lau, D. L., Yalla, V., and Casey, C., "Improved composite-pattern structured-light profilometry by means of postprocessing," *Opt. Eng.* **47**(9), 0972031–09720311 (2008).
7. Blais, F., "A review of 20 years of range sensor development," *Proceedings of SPIE-IS&T Electronic Imaging* **5013**, 62–76 (2003).
8. Srinivasan, H. C., Liu, H. C., and Halioua, M., "Automated phase measuring profilometry: a phase mapping approach," *Appl. Opt.* **24**, 185–188 (1985).
9. C., G., Hassebrook, G., L., and Lau, D. L., "Composite structured light pattern for three-dimensional video," *Opt. Express* **11**(5) (10 March 2003).
10. Halioua, M. and Liu, H., "Optical three-dimensional sensing by phase measuring profilometry," *Opt. Lasers Eng.* **11**, 185–215 (1989).
11. Li, J., Hassebrook, L. G., and Guan, C., "Optimized two-frequency phase measuring profilometry light sensor temporal noise sensitivity," *J. Opt. Soc. Am.* **20**, 106–115 (2003).
12. Song, J., Ho, Y. S., Lau, D. L., and Liu, K., "Universal phase unwrapping for phase measuring profilometry using geometry analysis," *Proc. SPIE* **10546**, 0B0–0B8 (2018).
13. Liu, K., Wang, Y., Lau, D., Hao, Q., and Hassebrook, L. G., "Dual-frequency pattern scheme for high-speed 3-d shape measurement," *Opt. Express* (1 March 2010).
14. Jiang, C., Lim, B., and Zhang, S., "Three-dimensional shape measurement using a structured light system with dual projectors," *Appl. Opt.* **57**(14), 3983–3990 (2018).
15. Lin, J., Jiang, K., and Chang, M., "A novel solution for camera occlusion in stereo vision technique," *Adv. Mech. Eng.* **2013**, 1–8 (2013).
16. O'Toole, M., Mather, J., and Kutulakos, K. N., "3d shape and indirect appearance by structured light transport," *IEEE Trans. Pattern Anal. Mach. Intell.* **38**(7), 1298–1312 (2016).
17. Wang, Y., Liu, K., Lau, D. L., Hao, Q., and Hassebrook, L. G., "Maximum snr pattern strategy for phase shifting methods in structured light illumination," *J. Opt. Soc. Am.* **27**(9), 1962–1971 (2010).
18. Xia, X. and Wang, G., "Phase unwrapping and a robust chinese remainder theorem," *IEEE Signal Processing Letters* **14**(4), 247–250.
19. Atcheson, B., Heide, F., and Heidrich, W., "Caltag: high precision fiducial markers for camera calibration," *Proceedings of the Vision, Modeling, and Visualization Workshop* (2010).
20. HDMI Licensing, LLC, *High-Definition Multimedia Interface Specification* (November 2009). Version 1.4.
21. Liu, K., Y. Wang, Lau, D. L., Hao, Q., and Hassebrook, L. G., "Gamma model and its analysis for phase measuring profilometry," *J. Opt. Soc. Am.* **27**(3), 553–562 (2010).